Physically based regularization of hydrogeophysical inverse problems for improved imaging of process-driven systems

E. K. Oware,[1] S. M. J. Moysey,[1] and T. Khan[2]

Received 29 April 2013; revised 24 July 2013; accepted 8 August 2013.

[1] We introduce a new strategy for integrating hydrologic process information as a constraint within hydrogeophysical imaging problems. The approach uses a basis-constrained inversion where basis vectors are tuned to the hydrologic problem of interest. Tuning is achieved using proper orthogonal decomposition (POD) to extract an optimal basis from synthetic training data generated by Monte Carlo simulations representative of hydrologic processes at a site. A synthetic case study illustrates that the approach performs well relative to other common inversion strategies for imaging a solute plume using an electrical resistivity survey, even when the initial conceptualization of hydrologic processes is incorrect. In two synthetic case studies, we found that the POD approach was able to significantly improve imaging of the plume by reducing the root mean square error of the concentration estimates by a factor of two. More importantly, the POD approach was able to better capture the bimodal nature of the plume in the second case study, even though the prior conceptual model for the POD basis was for a single plume. The ability of the POD inversion to improve concentration estimates exemplifies the importance of integrating process information within geophysical imaging problems. In contrast, the ability to capture the bimodality of the plume in the second example indicates the flexibility of the technique to move away from this prior process constraint when it is inconsistent with the observed ERI data.

Citation: Oware, E. K., S. M. J. Moysey, and T. Khan (2013), Physically based regularization of hydrogeophysical inverse problems for improved imaging of process-driven systems, *Water Resour. Res.*, *49*, doi:10.1002/wrcr.20462.

1. Introduction

[2] There is growing interest in using geophysical methods, such as electrical resistivity imaging (ERI), to investigate systems where the evolution of subsurface properties through space and time is constrained by physical, chemical, or biologic processes, such as the infiltration of water or transport of solutes in porous media. Subsurface imaging using ERI, however, usually requires the solution of an ill-posed inverse problem. While there are a variety of approaches addressing this issue in the inverse theory literature, Tikhonov regularization [*Tikhonov and Arsenin*, 1977] is commonly applied to ERI as it readily allows spatial constraints, such as smoothly varying property variations, to be enforced in subsurface images [e.g., *Daily and Ramirez*, 1995; *LaBrecque and Yang*, 2001; *Kemna et al*., 2002]. The spatial constraints applied in these inversions are typically generalized filters selected independently from the underlying processes affecting the target resistivity distribution (Figure 1a). In the context of imaging solute transport, it is well known that this regularization can lead to imaging artifacts causing problems with mass recovery and poor spatial resolution [e.g., *Singha and Gorlick*, 2005].

[3] In contrast, an emerging approach known as coupled inversion explicitly takes advantage of the dependence of geophysical properties on subsurface processes by using geophysical measurements to calibrate the parameters of a hydrologic model [e.g., *Rucker and Ferré*, 2004; *Ferré et al*., 2009; *Hinnell et al*., 2010]. Figure 1b illustrates how the coupled hydrologic and geophysical models can be considered as a single model with hydrologic parameters as inputs and geophysical responses as outputs. An advantage of the technique is that the coupled process model may have only a few parameters that control the detailed spatial and temporal evolution of hydrologic state variables in the subsurface, which in turn control the geophysical response. Coupled inversion can therefore be viewed as an implicit form of regularization that enforces a physics-based constraint on the inversion through the physical process simulator, e.g., the flow and transport model. A disadvantage of the approach, however, is that poor results may be obtained if the hydrologic model is subject to conceptual or structural errors or the geophysical model fails to capture the influence of nonhydrologic factors, such as background variations in resistivity.

[1]Environmental Engineering and Earth Sciences, Clemson University, Clemson, South Carolina, USA.
[2]Mathematical Sciences, Clemson University, Clemson, South Carolina, USA.

Corresponding author: S. M. J. Moysey, Environmental Engineering and Earth Sciences, Clemson University, Brackett Hall, Clemson, SC 29634, USA (smoysey@clemson.edu)

0043-1397/13/10.1002/wrcr.20462

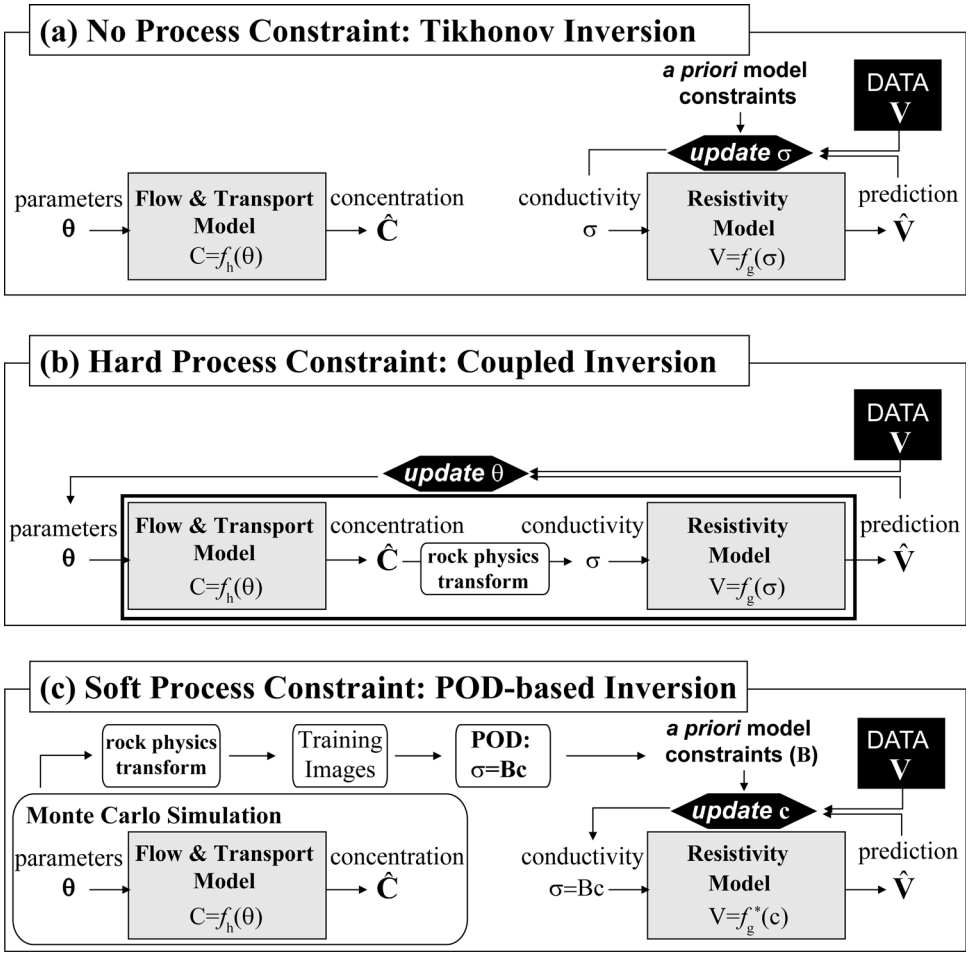

Figure 1. Schematic comparison of the (a) Tikhonov, (b) coupled, and (c) POD-based inversion strategies.

[4] We propose a new approach for physics-based regularization of inverse problems that is dependent on, but less restricted by, assumptions about subsurface processes compared to coupled inversion (Figure 1c). The approach uses proper orthogonal decomposition (POD) [e.g., *Banks et al*., 2000; *Kunisch and Volkwein*, 2003; *Rathinam and Petzold*, 2004; *Pinnau*, 2008] of a set of training data generated by Monte Carlo simulation of a hydrologic process to generate an optimal set of basis vectors for the imaging problem. These hydrologically "tuned" basis vectors are subsequently used within a basis-constrained inversion framework to obtain a resistivity image.

[5] To our knowledge, this work is the first use of POD to constrain geophysical inversions by physical process information. The use of training data to characterize spatially distributed patterns, however, is well established in a variety of fields in the geosciences. For example, the adoption of training images to infer spatial patterns in applications of multiple-point geostatistics [e.g., *Strebelle*, 2000] is increasingly common. *Moysey et al*. [2005] applied the training data concept by using geostatistically based Monte Carlo simulations of geophysical surveys to quantitatively capture and correct for spatially variable inversion artifacts associated with nonlinear imaging problems. Similarly, *Lehikoinen et al*. [2010] used Monte Carlo simulations of flow in a heterogeneous vadose zone to construct a statistical model of approximation errors resulting from the assumption of a homogenous medium, which they were subsequently able to utilize within a Kalman filter to improve resistivity imaging of water content changes. The use of simulations and training data to capture relevant information to constrain estimation and imaging problems is, therefore, already well-established in the literature. The key contribution of this work is establishing the use of POD to capture patterns from training data and efficiently integrate this information as a constraint within an inverse problem.

[6] In this paper, we compare the results of POD-based inversion to results obtained using standard Tikhonov regularization techniques and coupled inversion for a problem where ERI is used to image a solute plume. We investigate two distinct scenarios: one where the *a priori* understanding of flow and transport utilized in generating the training images for the inversions is correct and one where the training data are inconsistent with the actual processes.

2. POD-Based Imaging Strategy for ERI

[7] Details of ERI have been described by many authors [e.g., *Kemna et al*., 2002]. In principle, ERI surveys operate

by sequentially applying electric currents (I) to the subsurface using different pairs of current electrodes. The resulting voltage responses ($\mathbf{V_{obs}}$) are measured at potential electrodes and depend strongly on the electrical conductivity distribution of the subsurface $\boldsymbol{\sigma}$, where each element σ_m represents the electrical conductivity at spatial location x_m and electrical resistivity is the inverse of conductivity ($1/\sigma_m$). The inverse or "imaging" problem involves estimating the conductivity distribution $\boldsymbol{\sigma}$ from the voltage observations $\mathbf{V_{obs}}$. The Tikhonov objective function (equation (1)) addresses the ill-posed nature of the inverse problem by minimizing data misfit (E_d) subject to a model regularization constraint (E_m), where β is a trade-off parameter that balances these two objectives, $f_g(\cdot)$ represents the resistivity forward model, W is a spatial filter, and $\boldsymbol{\sigma_o}$ is a reference model or a priori estimate of conductivity.

$$E(\boldsymbol{\sigma}) = E_d + \beta E_m = \|\mathbf{V_{obs}} - f_g(\boldsymbol{\sigma})\|_2 + \beta\|\mathbf{W}(\boldsymbol{\sigma} - \boldsymbol{\sigma_o})\|_2. \quad (1)$$

[8] Basis-constrained inversions or subspace solutions [*Greenhalgh et al.*, 2006] restrict the inverse problem by assuming that a finite number of orthogonal spatial (or spatiotemporal) basis functions can be linearly recombined using an appropriate set of scaling coefficients $\mathbf{c}$ to reconstruct $\boldsymbol{\sigma}$ within a specified level of accuracy (i.e., approximation errors given by $\boldsymbol{\varepsilon} = \boldsymbol{\sigma}\text{-}\hat{\boldsymbol{\sigma}}$).

$$\boldsymbol{\sigma} \approx \hat{\boldsymbol{\sigma}} = \mathbf{Bc}. \quad (2)$$

[9] Here the N_p columns of the matrix $\mathbf{B}$ each contain a basis vector of length N_m that captures a particular spatial pattern needed to reproduce $\boldsymbol{\sigma}$. Given a known set of basis vectors, $\mathbf{B}$, the basis constrained inversion can be obtained by substituting the expansion of $\boldsymbol{\sigma}$ from equation (2) into an appropriate objective function, i.e., equation (1). A regularization filter $\tilde{\mathbf{W}}$ can be designed to place an a priori constraint directly on $\mathbf{c}$, e.g., to force coefficients of unnecessary basis vectors toward zero, or can be derived from spatial constraints on $\boldsymbol{\sigma}$ by projecting a desired spatial filter (i.e., $\mathbf{W}$) onto the basis (i.e., $\tilde{\mathbf{W}} = \mathbf{WB}$). Likewise, the reference model for the coefficients $\mathbf{c_o}$ can be obtained by projection of $\boldsymbol{\sigma_o}$ onto the basis. The modified function $f_g^*(\cdot)$ in equation (3) denotes that the electrical conductivity distribution must be reconstructed from the current estimate of $\mathbf{c}$ prior to applying the geophysical forward model $f_g(\cdot)$ to simulate the voltage responses. Given that only a few basis vectors may be needed to reconstruct $\boldsymbol{\sigma}$ within an acceptable level of error [*Loris et al.*, 2007; *Jin et al.*, 2011], the basis constrained inversion should generally be more stable than standard inversion strategies as fewer parameters need to be estimated (i.e., $N_p \ll N_m$). For this to be true, however, the basis vectors in $\mathbf{B}$ must be selected to allow for the reconstruction of $\boldsymbol{\sigma}$ in an efficient and accurate manner.

$$\begin{aligned} E(\mathbf{c}) &\approx \|\mathbf{V_{obs}} - f_g(\mathbf{Bc})\|_2 + \beta\|\mathbf{W}(\mathbf{Bc} - \mathbf{Bc_o})\|_2 \\ &= \|\mathbf{V_{obs}} - f_g^*(\mathbf{c})\|_2 + \beta\|\tilde{\mathbf{W}}(\mathbf{c} - \mathbf{c_o})\|_2 \end{aligned} \quad (3)$$

[10] Selection of an optimal basis constraint to minimize N_p for a particular subsurface process is not trivial. If a representative training data set is available, however, proper orthogonal decomposition (POD), which is also known as principal component analysis (PCA) or the Karhunen-Loève (KL) transform, can be used to derive an optimal orthogonal basis where the maximum amount of variability in the training data set (in a least squares sense) is captured with the fewest number of basis vectors [*Pinnau*, 2008]. While this decomposition is commonly used for image compression, pattern recognition, data analysis, and model order reduction in computational applications, it presents a challenge for subsurface imaging problems since high-resolution databases of real geologic environments do not exist. We suggest that this problem can be addressed by using Monte Carlo simulations of subsurface processes to produce a set of training data that captures general patterns of subsurface variability expected for $\boldsymbol{\sigma}$ at a particular site, which can subsequently be analyzed by POD (or equivalently PCA) to generate the basis.

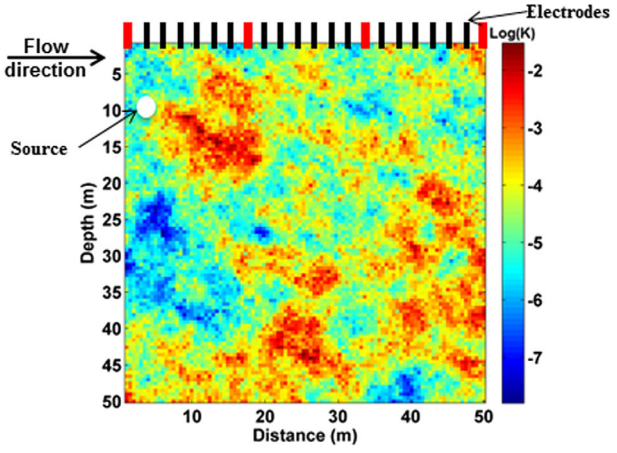

Figure 2. Schematic illustration of the experimental setup of the 2-D flow and transport in a random hydraulic conductivity field, along with the resistivity survey design. While the red electrodes served as both current and potential electrodes, the black electrodes were used exclusively as potential electrodes.

3. Methods

3.1. Simulation Overview for Test Scenarios

[11] We use a numerical test to compare the performance of ERI for imaging a solute plume using the POD approach versus standard Tikhonov methods and coupled inversion. The simulation domain for the tests consists of a 50 m × 50 m vertical cross section discretized into 0.5 m × 0.5 m cells. Refer to Figure 2 for an illustration of the experimental setup. The true target electrical conductivity distribution is obtained by simulating conservative solute transport through a heterogeneous hydraulic conductivity (K) field. The K field is generated using the algorithm SGSIM [*Deutsch and Journel*, 1998] for a lognormal hydrologic conductivity distribution with mean $\ln(K) = -4.6$ and variance $\ln(K) = 0.39$ to produce K values (in m/s) typical of a silty sand [*Freeze and Cherry*, 1979]. The spatial variability of the K field is described using an isotropic exponential variogram model with a correlation length of 25 m. The longitudinal dispersivity and porosity throughout the domain are fixed to values of 3.0 m and 0.3, respectively. A uniform unit hydraulic gradient drives mean horizontal

flow, while zero flux conditions were applied at the top and bottom boundaries of the domain.

[12] Two different transport scenarios are considered to test the ERI inversion techniques. In the first synthetic case, the solute originates from a single source location ($x = 2.5$ m, $z = 10$ m) with an initial fixed concentration of 2 g/L, thereby producing a unimodal plume at the time of imaging (see Figure 5a). In contrast, the solute originates from two distinct source zones in the second scenario ($x_1 = 2.5$ m, $z_1 = 7.5$ m, and $x_2 = 4$ m, $z_2 = 10$ m) each with an initial concentration of 2 g/L, thereby producing a bimodal plume as the imaging target (see Figure 5e). The initial background concentration in the aquifer was assumed to be uniform and equal to 140 mg/L. The total solute mass in the imaged area, including the background solutes, is therefore 1.6 kg for synthetic #1 and 1.8 kg for synthetic #2. The calculated values reported for the simulations in Table 1 are lower by approximately 1% and 3%, respectively, due to numerical errors in the transport simulation. All concentration boundary conditions were fixed to the background concentration throughout the simulation. Both the flow and transport simulations were performed using a finite-difference code written in MATLAB.

[13] Solute concentrations were converted to electrical conductivities using Archie's law: $\sigma(x) = \sigma_f n^m$, where n is porosity, the cementation exponent, m, was fixed to 1.3, and the electrical conductivity (S/m) of the fluid, σ_f, is assumed to be 1.5×10^{-4} times the solute concentration (given in mg/L) [*Lesmes and Friedman*, 2005]. Dipole-pole surveys were performed using a total of 22 electrodes deployed along the upper surface of the simulation domain (see Figure 2), four of which were utilized as current electrodes. The voltage potential resulting from six independent current injections was monitored at all remaining 20 electrodes, thereby producing 120 voltage measurements for each survey. All ERI forward simulations were performed using a modified version of the MATLAB code by *Pidlisecky et al*. [2007]. Notably, all of the ERI surveys are performed for the single observation time $t = 5.85$ years after the release of the solutes, i.e., the surveys do not represent time-lapse measurements.

3.2. Details for the ERI Inversions

[14] Standard Tikhonov regularization of the ERI data using spatial smoothness and model smallness constraints was performed using RESINVM3D [*Pidlisecky et al*., 2007]. An additional depth weighting factor equivalent to $1/z^2$ was used to penalize against changes in $\boldsymbol{\sigma}$ near the electrode locations as suggested by *Pidlisecky et al*. [2007]. The reference model $\boldsymbol{\sigma_0}$ was set to a constant value based on the initial solute concentration in the aquifer. The regularization parameter β was optimized by trial and error.

[15] Models of varying complexity can be utilized to represent flow and transport in a heterogeneous domain for the coupled inversion approach. We chose to use a very simple conceptual model given by the 2-D analytical solution for uniform lateral flow in equation (4) [*De Josselin De Jong*, 1958]. The use of this model implicitly assumes that the influence of the hydraulic conductivity heterogeneity on the solute can be captured by effective transport parameters, which is clearly not an accurate assumption since the second synthetic example has two solute sources, whereas the model assumes a single source. Regardless, we chose this simplified model to highlight strengths and weaknesses of the coupled inversion approach when model errors exist. We do not suggest that this is the only choice or even the optimal choice for providing accurate images of the plume using the coupled inversion approach.

$$C(x,z,t) = \frac{C_0 A}{4\pi t (D_L D_T)^{1/2}} \exp\left\{ -\frac{[(x - x_0) - v_x t]^2}{4 D_L t} - \frac{(z - z_0)^2}{4 D_T t} \right\} \tag{4}$$

[16] The initial tracer concentration C_0 is injected over an area A at location (x_0,z_0), such that the total solute mass in the system is given by $M = C_0 A$. The plume moves through the aquifer with a velocity v_x and the concentration at time t after tracer injection is $C(x,z,t)$. The longitudinal (D_L) and traverse (D_T) dispersion coefficients are defined as the product of velocity and dispersivity (α), i.e., $D_j = v_x \alpha_j$, where for this example, we chose $\alpha_L = 3.0$ m, and $\alpha_T = \alpha_L/3$. We recognize that this choice is not general and limits the ability of the model to reproduce a full range of plume aspect ratios, but the limitation does not impact the conclusions made in this study. Since dispersion is controlled by the plume velocity and transport time in this model, there are three parameters in equation (4) to be estimated: the mass of solute released from the source (M), the average lateral velocity of the plume (v_x), and the total time since the release of the plume (t). We used the trust-region-reflective optimization algorithm *lsqnonlin* in MATLAB [*Coleman and Li*, 1996] to perform this optimization subject to the constraint that all three model parameters are positive.

[17] Training data for the POD-based inversions were obtained by simulating flow and transport for the same conditions as the reference model with a single source zone, except that each simulation used an independent, randomly generated hydraulic conductivity realization. To account for the fact that the true spatial structure of the subsurface would normally be uncertain, the K realizations were simulated using four different correlation lengths (15, 20, 25, and 30 m). A total of 400 flow and transport simulations were performed. Each resulting concentration image was transformed to electrical conductivity using the form of Archie's law given earlier. Maps showing the mean and standard deviation of the training images are given in Figures 3a and 3b, respectively. Four sample realizations illustrating differences in the morphology of the plumes in the training images are also given (Figures 3c–3f).

[18] Prior to extraction of the basis vectors from the training data, the center of mass for each realization was calculated and the plumes were aligned to the true center of mass for the reference (i.e., true) plume. The plume centering step accounts for the translational dependence of the individual realizations in the training data and therefore reduces the number of realizations required to capture patterns that characterize an individual plume. We assume that the plume center of mass could generally be estimated directly from resistivity data based on the results of *Fowler and Moysey* [2011], who used numerical models to demonstrate that the effective plume velocity—which can be directly related to the center of mass—can be accurately

estimated with a single four-electrode array, and *Pidlisecky et al*. [2011], who used a moment-based inversion to improve plume imaging, though this work was demonstrated for cross-borehole ground-penetrating radar tomography, which has significantly different data sensitivities from ground-based resistivity surveys. The impact of our assumption is explored in the Discussion section of this paper, but we suggest investigation of robust methods for the estimation of the center of mass of a plume using resistivity surveys in complex, heterogeneous flow systems as a future research direction.

[19] Singular value decomposition of the training data set was used to calculate the POD basis vectors [*Pinnau*, 2008], of which the first 300 were retained as these could account for 99.6% of the variability in the training data set. Since only one coefficient needs to be estimated for each basis vector, this represents a 97% reduction in the number of parameters to be estimated in the inversion relative to the 10,000 pixels of the original σ image. Examples of the patterns captured from the training data are illustrated by the first 20 POD basis vectors given in Figure 4.

[20] The regularization operator $\tilde{\mathbf{W}}$ used in equation (2) consisted of two components. First, the same depth weighting function and spatial smoothness constraints on electrical conductivity used in the traditional Tikhonov regularization approach, i.e., $\mathbf{W}$, were applied here by projecting the previous regularization operator onto the basis vectors obtained from the training data, i.e., $\tilde{\mathbf{W}}_1 = \mathbf{WB}$. Second, a diagonal operator ($\tilde{\mathbf{W}}_2$) containing the inverse of the singular values derived from the SVD of the training data was added to $\tilde{\mathbf{W}}_1$ to force the basis coefficients, i.e., $\mathbf{c}$, toward zero with a preference to retain the basis vectors most representative of the training data. This constraint enforces a bias to produce ERI results that are similar to the mean of the training images. The overall regularization operator used in equation (2) for the basis constrained inversion is therefore $\tilde{\mathbf{W}}^T\tilde{\mathbf{W}} = \tilde{\mathbf{W}}_1{}^T\tilde{\mathbf{W}}_1 + \gamma\tilde{\mathbf{W}}_2 = \mathbf{B}^T\mathbf{W}^T\mathbf{WB} + \gamma\tilde{\mathbf{W}}_2$, where the parameter γ is an additional regularization parameter providing a relative weighting between these two terms. The reference model $\mathbf{c_o}$ was obtained from projection of $\boldsymbol{\sigma_o}$ onto $\mathbf{B}$.

[21] Estimates of electrical conductivity obtained by each inversion technique were subsequently back converted to concentrations according to Archie's law, as presented earlier. A variety of metrics were then evaluated for each image to quantitatively compare the inversion strategies. The metrics used here include root-mean-square error (RMSE) of the estimated concentrations, maximum (peak) plume concentration, and total plume mass (zeroth-order spatial moment).

4. Results and Discussion

[22] A comparison of the electrical conductivity images estimated by each of the three different inversion schemes is given in Figure 5 and comparisons of the true and estimated concentrations are given in Figure 6. A summary of the metrics used to compare the estimated results to the true plume is given in Table 1.

[23] For synthetic #1, i.e., the scenario with a single solute source and unimodal plume, the traditional Tikhonov inversion with smoothness and smallness constraints produces an overly smooth and damped image compared to the true plume (Figure 5b). As a result, the estimated concentrations are low compared to their true values (Figure 6a), resulting in a high concentration RMSE of 70 mg/L. The peak concentration of the plume is also greatly underestimated at 380 mg/L versus 1180 mg/L for the true plume, i.e., a 68% error. The total mass of the estimated plume is 1.56 kg versus 1.58 kg, thus yielding only a 1% error for this example. In this case, the low mass error is presumably a result of the fact that the smoothness constraint in the Tikhonov inversion forces the estimated plume to spread out over a much larger region of the subsurface than the true plume, which compensates for the low concentration estimates.

Table 1. Summary of Metrics for Concentration and Conductivity Values Estimated by ERI for the Single Source (Synthetic #1) and Dual Source (Synthetic #2) Transport Scenarios[a]

		Total Mass (kg)	Max Value		RMSE	
			Conc. (g/L)	Log(σ)	Conc. (g/L)	Log(σ)
Synthetic #1	True Plume	1.58	1.18	−3.30	–	–
	TI Mean	1.56	1.14	−3.34	0.08	0.18
	Tikhonov	1.56	0.38	−4.43	0.07	0.17
	Coupled	1.51	0.51	−4.14	0.07	0.17
	POD	1.60	1.45	−3.09	0.03	0.07
Synthetic #2	True Plume	1.75	1.79	−2.88	–	–
	TI Mean	1.56	1.14	−3.34	0.13	0.28
	Tikhonov	1.63	0.93	−3.53	0.12	0.25
	Coupled	1.62	0.63	−3.93	0.12	0.25
	POD	1.70	1.64	−2.97	0.08	0.12

[a]TI Mean refers to estimates obtained by taking the mean of the training images obtained by Monte Carlo flow and transport simulation, which are independent of the geophysical data.

[24] Coupled inversion does a better job capturing the compact morphology of the plume for synthetic #1 (Figure 5c). The limitations of the analytical transport model are clear, however, as the irregular shape and off-axis rotation of the true plume cannot be reproduced. We emphasize that these particular issues are limitations of the analytical model selected for this example, not inherent limitations of the coupled inversion approach. Regardless, the analytical

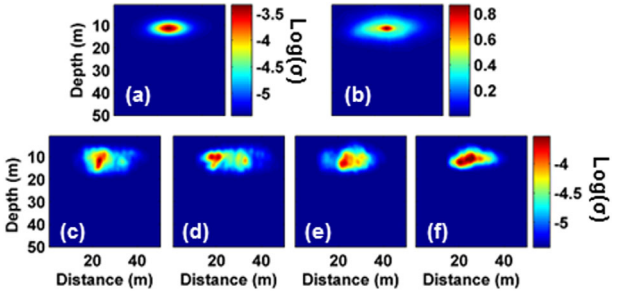

Figure 3. (a) Mean and (b) standard deviation maps of the log-electrical conductivity for the 400 images in the training data. Four sample realizations are shown in c-f to illustrate the variability in the shape of the plumes observed in the realizations. Note that the realizations have been shifted such that the center of mass of each plume is aligned with the center of mass of the true plume.

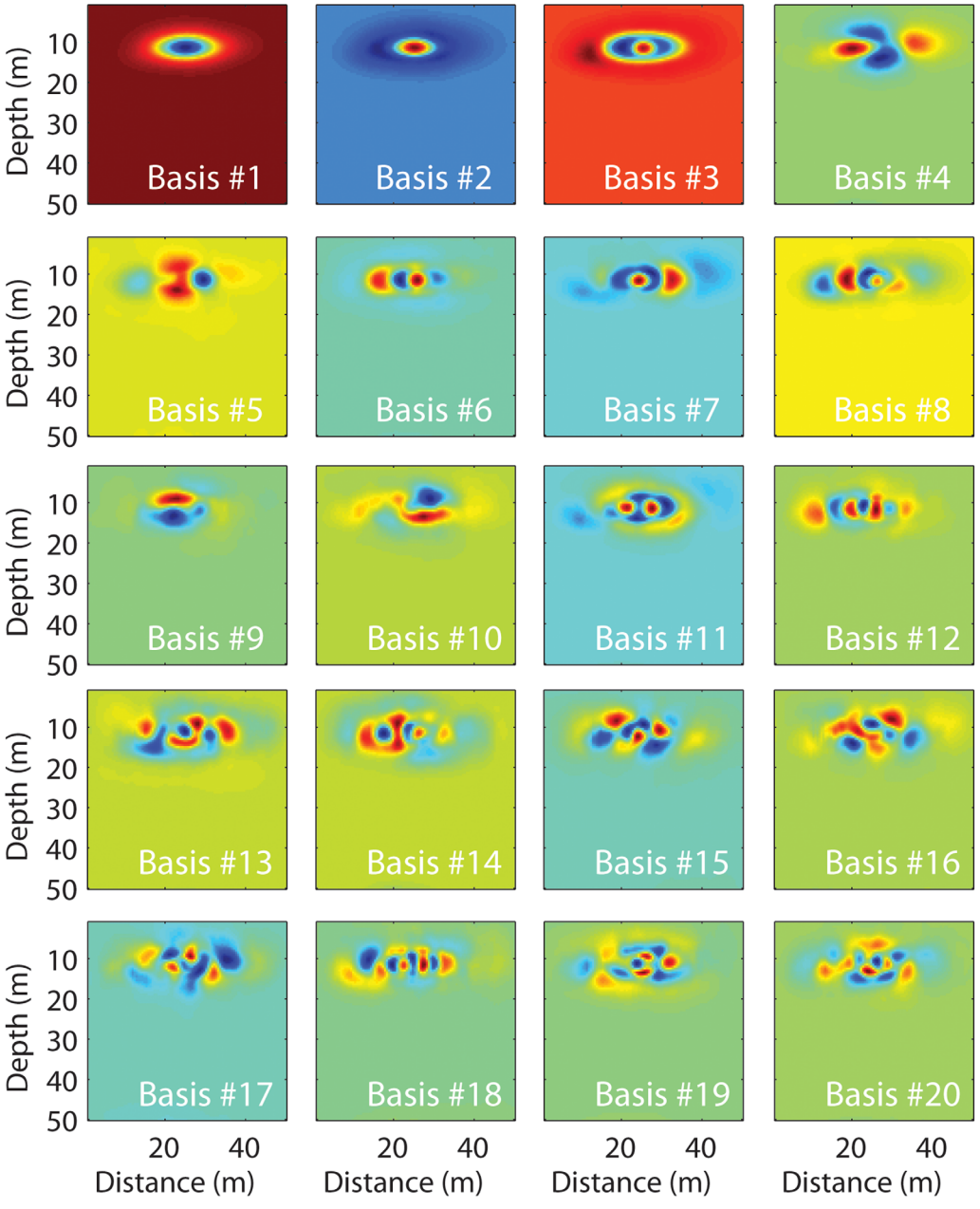

Figure 4. Examples of the top 20 most important POD basis images extracted from the training data set.

model facilitates localization of the solute mass within a distinct plume, thus allowing the estimate of the peak concentration to increase to 510 mg/L, which yields an error of 57% (a decrease of 11% compared to the Tikhonov approach). The average concentration misfit as quantified by the RMSE is similar to that observed for the Tikhonov inversion (70 mg/L), but the error for the estimated total solute mass (M = 1.51 kg) is slightly higher in this case.

[25] The POD-based inversion provides the best overall estimate of both plume morphology and concentrations (Figures 5d and 6c). The peak plume concentration estimated by the POD approach is 1450 mg/L, which is an overestimate of the true peak concentration by 23%. From Figure 6c, however, it is clear that only a small percentage of the 10,000 pixels in the image are significantly overestimated, whereas the concentration underestimation that occurred for the Tikhonov and coupled inversions was more systematic. The total mass is also slightly overestimated, but with an error similar in magnitude to the other two inversion approaches (i.e., 1%). The concentration RMSE in this case is only 30 mg/L, however, which indicates a marked improvement in the overall reproduction of the solute plume concentrations compared to either the Tikhonov or coupled inversion approach.

[26] Given that the POD inversion is dependent on the simulated training images to obtain the basis functions, it is important to evaluate whether the ERI data actually improved the concentration estimates or if the POD inversion results simply reflect the mean behavior of the training data. In other words, we ask the question "Could an equally

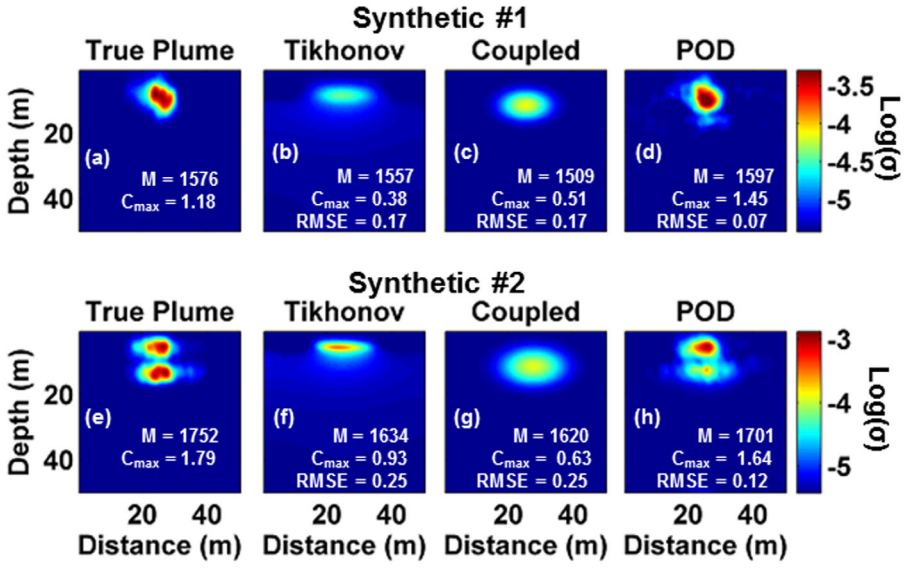

Figure 5. (a and e) True and estimated conductivity tomograms for (b and f) Tikhonov regularization with spatial constraints, (c and g)coupled inversion, and (d and h) POD-based inversion for transport scenario 1 (unimodal plume; top row) and scenario 2 (bimodal plume; bottom row). Inset on each plot is the root mean square error (RMSE), maximum estimated concentration (Peak; mg/L), and total estimated mass of solute (Mass; g).

good estimation result be obtained using stochastic simulation alone?" Comparing the image obtained by taking the mean of the training realizations (Figure 3a) to the true plume (Figure 5a), it is apparent that the resulting images are substantially different. The RMSE obtained for the mean of the concentration realizations is 80 mg/L, which is higher than that obtained for any of the other ERI-based imaging methods. The total mass and peak concentration estimated from the mean of the realizations, however, are similar to their true values. The high degree of misfit indicated by the RMSE, but good match for the other two plume metrics suggests that the realizations capture some general characteristics of the true plume that are independent of the specific spatial distribution of the solute concentrations. Including the ERI data in the estimation problem focuses the image toward the specific subsurface distribution of concentration for the true plume.

[27] As pointed out earlier, we made the assumption in this work that it would be possible to shift the training images to the true center of mass of the plume prior to

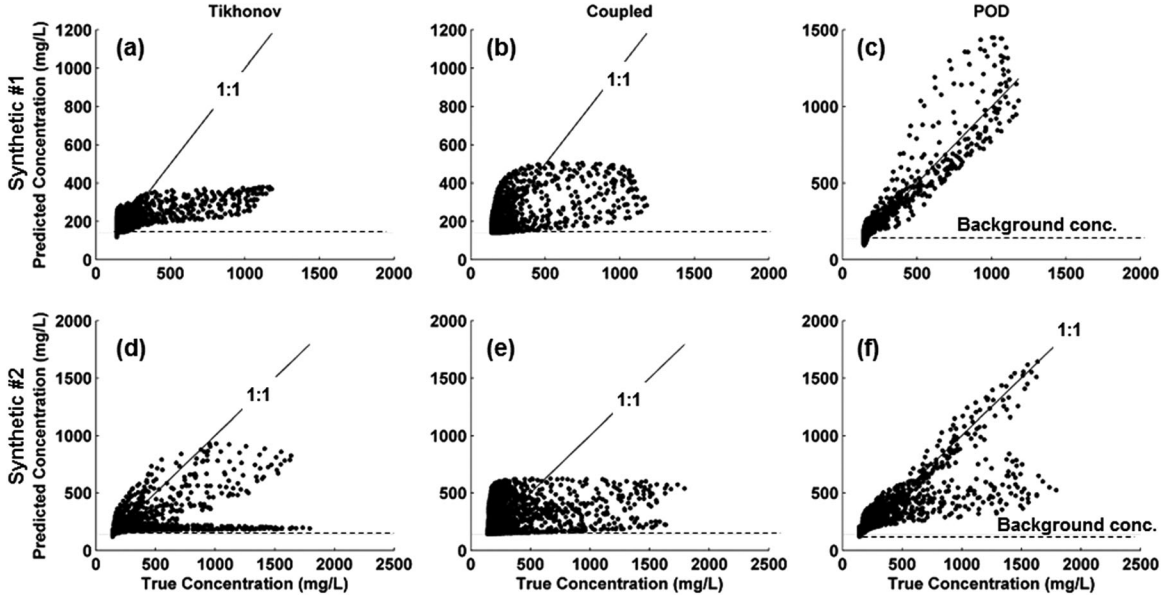

Figure 6. (a and d) Scatterplots showing accuracy of concentration estimates for Tikhonov regularization with spatial constraints, (b and e) coupled inversion, and (c and f) POD-based inversion. The dashed line in each figure shows the background concentration of the aquifer (140 mg/L).

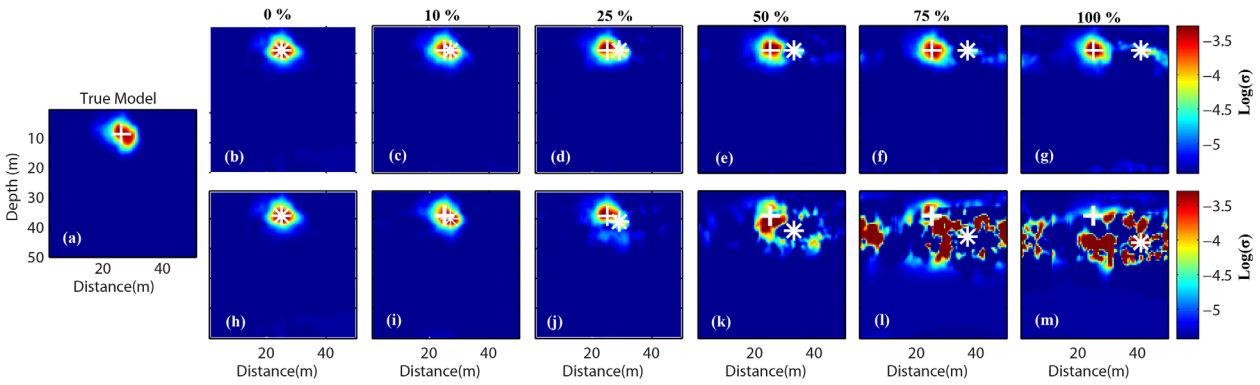

Figure 7. (a) True plume versus estimated conductivity tomograms obtained when the center of mass of the training images used for the POD inversion is shifted (first row, b–g) longitudinally and (second row, h–m) diagonally. The white + in each image denotes the position of the center of mass of the true plume, whereas the * indicates the center of mass used to shift the training images; the title above each column indicates the magnitude of the shift as a percentage of the plume width.

performing the POD analysis. To assess the significance of this assumption, we explored the performance of the POD inversion under varying degrees of error in the estimated center of mass. To account for differences in the lateral and vertical sensitivity of resistivity data, we considered cases where the estimated center of mass was shifted either laterally or diagonally relative to the true center of mass for the reference plume. In an effort to gain quantitative insight into how the magnitude of the positioning error affected the imaging results, we tested cases where the training images were shifted by 10, 25, 50, 75, and 100% of the width of the plume (as quantified by the second spatial moment of the plume [*Freyberg*, 1986]).

[28] Overall, the POD inversion appears to be relatively robust to errors in the plume's estimated center of mass. Figure 7 qualitatively illustrates that lateral shifts in the plume center of mass are minor for synthetic #1 until the training data are shifted by an entire plume-width. In contrast, the image degrades significantly when the plume is shifted by 50% of its width in the diagonal direction. These results are shown quantitatively in Figure 8 for both synthetic #1 and #2, where the RMSE of the estimated log conductivity image does not become greater than that obtained using either the Tikhonov or coupled inversion strategies until the training images are shifted by at least 25% of the reference plume's width. It is also clear from this plot that lateral errors in the plume center of mass generally produce small increases in the imaging error.

[29] Synthetic #2 was a more complicated problem in the sense that the two solute sources produced a bimodal

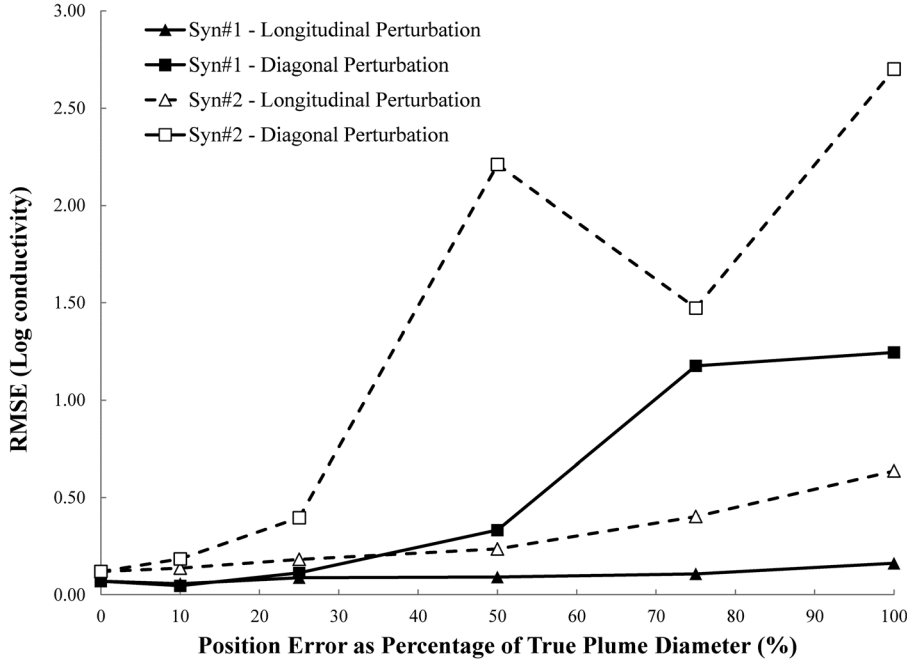

Figure 8. Change in RMSE for the estimated conductivity images as a function of the position error for the plume center of mass used to shift the training images prior in the POD analysis.

plume (Figure 5e). Since the Tikhonov inversion makes no assumptions about the underlying processes generating the target conductivity distribution, there is no conceptual inconsistency introduced in the imaging problem compared to synthetic #1. The resistivity survey, however, consisted of only 120 measurements over a limited range of electrode separations. The sensitivity of the resistivity measurements for this data poor survey is therefore limited for imaging the deeper part of the plume in this particular example. The result is that the upper portion of the plume is still not well estimated and the lower part is completely missed by the survey (Figure 5f). The plume metrics from Table 1 now indicate a significant underestimation of total mass (7%), peak concentration (48%), and high RMSE (120 mg/L) for the Tikhonov-based estimates.

[30] The coupled inversion approach produces similarly poor estimation results based on the concentration metrics from Table 1 (7% error in total mass, 65% error in peak concentration, and 120 mg/L concentration RMSE). Figure 4g shows that the reason for this poor estimation is somewhat different than the Tikhonov case. The estimated plume for the coupled inversion has shifted downward and grown to reflect the greater size of the true bimodal plume. Since the analytical model used in the inversion only allows for plumes with a single peak, the coupled inversion produced a result that spread the solute mass over a larger part of the subsurface to account for the larger distribution of mass of the true plume.

[31] An improved estimate of the plume could, of course, be achieved by coupled inversion if the transport model was updated to allow for bimodal plumes, e.g., by using superposition of two unimodal plumes or increasing the degree of complexity by using a numerical transport model with multiple sources and heterogeneous flow and transport parameters. The point of our example, however, is to very simply illustrate the problem that occurs when the hydrologic conceptual model is inaccurate, not to illustrate which method can produce the best possible image when the conceptual model is correct. Our belief is that coupled inversion is the optimal approach for inversion when an accurate hydrologic model is available and estimating the value of the model parameters is the goal, though research is still continuing on this front.

[32] The training images used for the POD analysis were also based on the incorrect conceptual model of a single solute source. The fact that the concentration realizations, which are the same ones used in synthetic #1, capture the behavior of the incorrect conceptual model is made clear by comparing the mean image in Figure 3a to the true plume in Figure 5e. Likewise, the plume metrics for the training image realizations indicate a significant underestimation of mass 11% error) and peak concentration (36% error) because the second plume was not included within the conceptual model used to generate the realizations.

[33] Despite the incorrect conceptual model used to generate the training images for synthetic #2, the POD inversion result suggests that the ERI data are able to compensate to obtain a much improved estimate for the bimodal plume. The POD inversion is able to recover 97% of the total solute mass, underestimates the peak concentration of the plume by only 8%, and has a concentration RMSE of 120 mg/L, which is a factor of two less than the other methods. More importantly, the plume image in Figure 5h suggests that the assumption of a unimodal plume for the distribution of solute mass may not be appropriate. Though the bimodal plume is not fully reproduced, the imaging result does suggest that a reconceptualization of the underlying transport model would be appropriate. In this way, the POD approach shows flexibility in moving estimates away from our preconceptions, while still providing the ability to account for the morphologic characteristics imparted to the target by the driving physical processes.

5. Conclusions

[34] In this paper, we presented a new approach for integrating process-based information within geophysical inversions. Specifically, proper orthogonal decomposition (POD) was used to extract a set of basis vectors for the imaging problem that are "tuned" for a particular hydrologic problem of interest using Monte Carlo simulation. We explored the approach here using two synthetic examples, one with a single source zone and one with two source zones leading to the formation of a bimodal plume.

[35] Although the examples presented here are simple, they effectively illustrate the potential of the POD-based inversion strategy for enforcing physical or biogeochemical process constraints on geophysical inverse problems. When the conceptual transport model was correct in the first scenario, both coupled and POD-based inversions are able to produce better estimates of the target plume than the Tikhonov inversion. In contrast, the coupled inversion failed when the conceptual model of transport was incorrect in the second scenario. The POD inversion, however, captured the bimodality of the plume by constraining the inversion by a priori process information while retaining the flexibility to honor observed geophysical data.

[36] The POD inversion is therefore a promising intermediate approach for enforcing physics-based regularization in a wide array of geophysical inverse problems. When a process controlling the imaging target is not known or highly uncertain, the POD approach is unlikely to perform better than standard Tikhonov methods since the range of results captured by a process simulator could be large. In contrast, when processes at a site are known and well understood, the coupled inversion approach can be an excellent choice for parameterizing models of the flow system. The POD approach is therefore an intermediate strategy that should be applied in cases where the processes are generally known, but not fully defined.

[37] Additional research is needed to more fully evaluate how uncertainty in site processes affects the overall performance of the POD approach compared to existing Tikhonov and coupled inversion techniques. This work, however, provides a first introduction to the technique and the synthetic examples illustrate how it may perform for real imaging problems. Many questions remain to be addressed in the future, however, such as how robust the technique is in the presence of noisy data? what is the role of data coverage on estimation accuracy? how uncertain and/or nonlinear a hydrologic model must be before the POD approach will not work? how will performance be affected by considering a three-dimensional system? and what methods may be used for efficient solutions to

estimate the POD coefficients and assess the imaging results. We therefore feel that the POD methodology provides a novel new approach for geophysical imaging that is ripe for future exploration.

[38] **Acknowledgments.** We thank one anonymous reviewer, Peter Bauer-Gottwein, Ty Ferre, and James Irving for their thoughtful reviews and suggestions that were used to improve this manuscript. This material is based upon work supported by the National Science Foundation under grants EAR-1151294 and DMS-0915214.

References

Banks, H. T., M. L. Joyner, B. Wincheski, and W. P. Winfree (2000), Nondestructive evaluation using a reduced-order computational methodology, *Inverse Probl.*, *16*, 929–945.

Coleman, T. F., and Y. Li (1996), An interior, trust region approach for nonlinear minimization subject to bounds, *SIAM J. Optim. 6*, 418–445.

Daily, W., and A. Ramirez (1995), Electrical-resistance tomography during in-situ trichloroethylene remediation at the Savanna river site, *J. Appl. Geophys.*, *33*, 239–249.

De Josselin De Jong, G. (1958), Longitudinal and transverse diffusion in granular deposits, *Trans. AGU*, *39*, 1–6.

Deutsch, C. V., and A. G. Journel (1998), *GSLIB: Geostatistical Software Library and User's Guide*, Oxford Univ. Press, New York.

Ferré, T., L. Bentley, A. Binley, N. Linde, A. Kemna, K. Singha, K. Holliger, J. A. Huisman, and B. Minsley (2009), Critical steps for the continuing advancement of hydrogeophysics, *EOS Trans. AGU*, *90*(23), 200, doi:10.1029/2009Eo230004.

Fowler, D. E., and S. M. J. Moysey (2011), Estimation of aquifer transport parameters from resistivity monitoring data within a coupled inversion framework, *J. Hydrol.*, *409*, 545–554, doi:10.1016/j.jhydrol. 2011.08. 063.

Freeze, R. A., and J. A. Cherry (1979), *Groundwater*, 604 pp., Prentice-Hall, Englewood Cliffs, N. J.

Freyberg, D. L. (1986), A natural gradient experiment on solute transport in a sand aquifer: 2. Spatial moments and the advection and dispersion of nonreactive tracers, *Water Resour. Res.*, *22*(13), 2031–2046, doi: 10.1029/WR022i013p02031.

Greenhalgh, S. A., Z. Bing, and A. Green (2006), Solutions, algorithms and inter-relationships for local minimization search geophysical inversion, *J. Geophys. Eng.*, *3*, 101–113, doi:10.1088/1742–2132/3/2/001.

Hinnell, A. C., T. P. A. Ferre, J. A. Vrugt, J. A. Huisman, S. Moysey, J. Rings, and M. B. Kowalsky (2010), Improved extraction of hydrologic information from geophysical data through coupled hydrogeophysical inversion, *Water Res. Res.*, *46*, W00D40, doi:10.1029/2008WR007060.

Jin, B., T. Khan, and P. Maass (2011), A reconstruction algorithm for electrical impedance tomography based on sparsity regularization, *Int. J. Num. Meth. Eng.*, *89*, 337–353, doi:10.1002/nme.3247.

Kemna, A., J. Vanderborght, B. Kulessa, and H. Vereecken (2002), Imaging and characterisation of subsurface solute transport using electrical resistivity tomography (ERT) and equivalent transport models, *J. Hydrol.*, *267*, 125–146.

Kunisch, K., and S. Volkwein (2003), Galerkin proper orthogonal decomposition for a general equation in fluid dynamics, *SIAM J. Numer. Anal.*, *40*(2), 492–515.

LaBrecque, D. J., and X. Yang, (2001), Difference inversion of ERT data: A fast inversion method for 3-D in-situ monitoring, *J. Environ. Eng. Geophys.*, *6*(2), 83–89.

Lehikoinen, A., J. M. J. Huttunen, S. Finsterle, M. B. Kowalsky, and J. P. Kaipio (2010), Dynamic inversion for hydrogeophysical process monitoring with electrical resistance tomography under model uncertainties, *Water Resour. Res.*, *46*, W04513, doi:10.1029/2009WR 008470.

Lesmes, D. P., and S. P. Friedman (2005), Relationships between the electrical and hydrogeological properties of rocks and soils, in *Hydrogeophysics*, edited by Y. Rubin and S. S. Hubbard, pp. 87–128, Springer, Dordrecht, Netherlands.

Loris, I., G. Norlet, I. Daubechies, and F. A. Dahlen (2007), Tomographic inversion using l_1-norm regularization of wavelet coefficients, *Geophys. J. Int.*, *170*, 359–370, doi:10.1111/j.1365-246X.2007.03409.x.

Moysey, M. S., K. Singha, and R. Knight (2005), A framework for inferring field-scale rock physics relationship through numerical simulation, *Geophys. Res. Lett.*, *32*, L08304, doi:10.1029/2004GL022152.

Pidlisecky, A., E. Haber, and R. Knight (2007), RESINVM3D: A 3D resistivity inversion package, *Geophysics*, *72*(2), H1–H10, doi:10.1190/ 1.2402499.

Pidlisecky, A., K. Singha, and F. D. Day-Lewis (2011), A distribution-based parameterization for improved tomographic imaging of solute plumes, *Geophys. J. Int.*, *187*, 214–224, doi:10.1111/j.1365-246X.2011. 05131.x.

Pinnau, R. (2008), Model reduction via proper orthogonal decomposition, in *Model Order Reduction: Theory, Research Aspects and Applications*, edited by W. H. A. Schilder and H. van der Vorst, pp. 96–109, Springer, New York.

Rathinam, M., and L. R. Petzold (2004), A new look at proper orthogonal decomposition, *SIAM J. Numer. Anal.*, *41*(5), 1893–1925.

Rucker, D. F., and T. P. A. Ferré (2004), Parameter estimation for soil hydraulic properties using zero-offset borehole radar: Analytical method, *Soil Sci. Soc. Am. J.*, *68*, 1560–1567.

Singha, K., and S. M. Gorelick (2005), Saline tracer visualized with three-dimensional electrical resistivity tomography: Field-scale spatial moment analysis, *Water Resour. Res.*, *41*, W05023, doi:10.1029/ 2004WR003460.

Strebelle, S., 2000, Sequential simulation drawing structures from training images, PhD dissertation, 187 pp., Stanford Univ., Stanford, Calif.

Tikhonov, A. N., and V. Y. Arsenin (1977), *Solutions of Ill-Posed Problems*, John Wiley and Sons, New York.